Observation of Confinement-Induced Resonances in a 3D Lattice

Deborah Capecchi[1], Camilo Cantillano[1], Manfred J. Mark[1,2], Florian Meinert[3], Andreas Schindewolf[4,5], Manuele Landini[1], Alejandro Saenz[6], Fabio Revuelta[7], and Hanns-Christoph Nägerl[1]

[1]*Institut für Experimentalphysik und Zentrum für Quantenphysik, Universität Innsbruck, 6020 Innsbruck, Austria*
[2]*Institut für Quantenoptik und Quanteninformation, Österreichische Akademie der Wissenschaften, 6020 Innsbruck, Austria*
[3]*5.Physikalisches Institut and Center for Integrated Quantum Science and Technology, Universität Stuttgart, 70569 Stuttgart, Germany*
[4]*Max-Planck-Institut für Quantenoptik, 85748 Garching, Germany*
[5]*Munich Center for Quantum Science and Technology, 80799 München, Germany*
[6]*Institut für Physik, Humboldt-Universität zu Berlin, 12489 Berlin, Germany*
[7]*Grupo de Sistemas Complejos, Escuela Técnica Superior de Ingeniería Agronómica, Alimentaria y de Biosistemas,
Universidad Politécnica de Madrid, 28040 Madrid, Spain*

We report on the observation of confinement-induced resonances for strong three-dimensional (3D) confinement in a lattice potential. Starting from a Mott-insulator state with predominantly single-site occupancy, we detect loss and heating features at specific values for the confinement length and the 3D scattering length. Two independent models, based on the coupling between the center-of-mass and the relative motion of the particles as mediated by the lattice, predict the resonance positions to a good approximation, suggesting a universal behavior. Our results extend confinement-induced resonances to any dimensionality and open up an alternative method for interaction tuning and controlled molecule formation under strong 3D confinement.

Cold atoms are a well-established platform for quantum simulation and computation [1,2]. They allow for the realization of strongly correlated quantum many-body phases [3] and hold promise for the investigation of dynamical processes in correlated quantum matter [4] with exquisite parameter control. Cold atoms come with two advantageous and enabling features: external potentials that can be flexibly created by optical means, e.g., optical lattices [5,6], and interatomic interactions that can be tuned almost at will, via magnetic Feshbach resonances (FRs) [7]. These features have been instrumental to a multitude of spectacular results, e.g., on the superfluid-to-Mott-insulator quantum phase transition [8,9] and the Bose-Einstein-condensation-to-Bardeen-Cooper-Schrieffer crossover [10]. Besides inter-action tuning, FRs serve as an entrance door to the world of ultracold molecules [11,12], with great promise for ultracold chemistry [13], precision measurements [14], and dipolar many-body physics [15]. For a FR to occur, the free scattering state of two atoms needs to be brought to degeneracy with a molecular bound state. In most applications, a variable external magnetic field tunes the energy difference, inducing the resonance.

Tight external confinement as provided by, e.g., a lattice can also lead to a dramatic modification of the atoms' scattering properties [16–23]. Confinement-induced resonances (CIRs) occur if the typical length scale of the confining potential, e.g., the harmonic-oscillator length a_h, and the 3D s-wave scattering length a_s assume similar values. CIRs come in two flavors: elastic (ECIR) and inelastic (ICIR). ECIRs emerge if the effective 1D or 2D interaction strength diverges at a specific *unique* value of the ratio of these two length scales [16–18]. On the other hand, an infinite series of ICIRs [23–26] emerges, if center-of-mass motion (CM) and relative motion (RM) are coupled [20,27–29] and thus molecular formation [30] or dissociation becomes possible by transferring the binding energy from one degree of freedom to the other. The occurrence of such a coupling is a ubiquitous phenomenon. It is absent only in very idealized cases like two identical atoms in a strictly harmonic or square-well potential. Already the slight anharmonicity of a lattice is sufficient to induce a coupling and thus an ICIR. In fact, ICIRs can also occur for other trapped particles like electrons in quantum dots or quasiparticles like excitons [31].

The positions of ECIRs and ICIRs can be tuned by varying a_h or a_s. They may be used, similar to FRs, to set the effective interparticle interaction. For dipolar particles, ICIRs can be tuned additionally by varying the dipolar interaction [25]. Because of molecule formation, ICIRs may lead to loss. Remarkably, ICIRs allow also for the

tuning of the coupling strength of the resonance itself by changing the confinement's anharmonicity.

Experimentally, controlling interactions on ECIRs in 1D has been used, e.g., to access the super-Tonks Girardeau regime [32,33], to map out three-body correlations [34], and to evade thermalization [35]. ICIRs have been used to coherently produce molecules [30]. ECIRs and ICIRs have been observed in the 1D-to-2D crossover [36,37], in mixed dimensionality [39], and in 2D [40].

In this Letter, we experimentally detect ICIRs in 0D as a result of strong 3D confinement. Interestingly, we find the resonances starting from a Mott-insulator state with predominantly single-site occupancy, a situation for which one would expect at first glance a strong suppression of atom-atom scattering. We employ Cs atoms in the hyperfine $(F, m_F) = (3, 3)$ ground state, which features wide tunability for a_s due to a combination of broad and narrow FRs [41], as shown in Fig. 1(a). We take data with two different experimental setups, one ($E1$) [42] for tuning a_s on a broad background, and the other ($E2$) [43] for tuning near a comparatively narrow FR.

We model our data by two complementary approaches based on previous work [23,24], named in the following $M1$ and $M2$ [44], both providing an approximate solution of the two-body problem in the presence of the 3D-lattice potential. The potential energy of two atoms is given by $V(\mathbf{r}_1, \mathbf{r}_2) = V_{RM}(\mathbf{r}) + V_{CM}(\mathbf{R}) + W(\mathbf{r}, \mathbf{R})$, where $\mathbf{r}_1$ ($\mathbf{r}_2$) is the position of atom 1 (2) and $\mathbf{r}$ ($\mathbf{R}$) is the RM (CM) coordinate. For $M1$, V_{RM} is Taylor expanded to order r^6 (sextic potential), and the eigenenergies of the RM are found perturbatively employing the solution for two particles in a harmonic trap interacting via a pseudopotential [45]. The CM is solved exactly given the lattice potential. In particular, $M1$ accounts for the full lattice bandwidth, without imposing any restriction on the quasimomentum, resulting in an allowed range for each crossing between the levels associated with an ICIR rather than in a fixed condition [44]. As a consequence, $M1$ (as opposed to $M2$) can describe the motion of the atoms moving as pairs through the lattice, as illustrated in Fig. 1(b) [46]. Finally, the coupling term W, which originates from the anharmonicity of the lattice potential, is treated perturbatively, leading to avoided crossings. For $M2$, the terms relative to the lattice-well potential are also expanded and the solution is found numerically, with the interaction between the atoms being described by an *ab initio* potential [44]. The coupling term W emerges from the expansion and is included in the numerical treatment. The results of $M2$ for the sextic Taylor expansion, which implies in the case of the RM that the two particles occupy the same well, have been assessed by comparison with a double-well description of the system provided by a twelve-order Taylor expansion (see Ref. [44]). Finally, $M2$ (in contrast to $M1$) allows for the description of anisotropic settings.

In both models, the RM eigenfunctions can be classified by two families of states: There are molecular bound states,
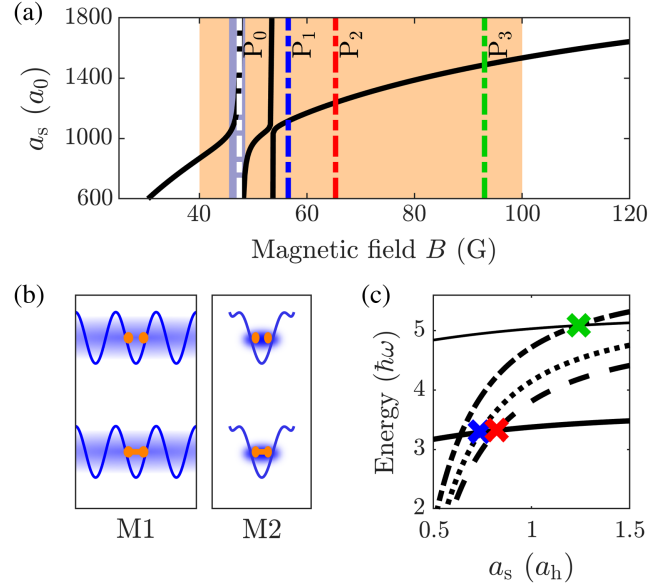

FIG. 1. (a) Scattering length a_s for Cs $(F, m_F) = (3, 3)$ as a function of B (solid black line) [41], with two narrow FRs at 47.8 G and 53.8 G. Orange (blue) shaded area corresponds to the interval used in experiment $E1$ ($E2$). The dashed lines labeled P_0, P_1, P_2, and P_3 mark the positions of the resonant features observed in $E1$. (b) Schematic representation of the CM states involved in the ICIRs: trap (upper) and bound (lower) state according to each model of the atom pair [23]. For model $M1$ ($M2$) the trapping potential is given by the lattice (sextic) potential. Initially, both atoms are in the same lattice site in a trap state (separated orange circles), while the CM (blue area) can be spread ($M1$) or localized ($M2$). ICIRs occur if the anharmonicity of the trapping potential couples the trap state to the least-bound state (connected orange circles) with some CM excitations. (c) Schematic energy diagram for varying a_s in units of a_h for isotropic trapping. The thick and thin solid lines correspond to $\psi_t^{RM}\phi_{iso}^{CM}(0, 0, 0)$ and $\psi_t^{RM}\phi_{iso}^{CM}(2, 0, 0)$, respectively, whereas the dashed, dotted, and dashed-dotted curves represent $\psi_b^{RM}\phi_{iso}^{CM}(4, 0, 0)$, $\psi_b^{RM}\phi_{iso}^{CM}(2, 2, 0)$, and $\psi_b^{RM}\phi_{iso}^{CM}(6, 0, 0)$, respectively. Intersections causing the ICIRs of the present work are indicated by crosses.

the most loosely bound denoted as ψ_b^{RM}. Then, there are higher-lying unbound states determined by the trap. These states energetically lie in the dissociation continuum in the absence of the external potential, and become discrete trap states in a few-well potential or bands in a lattice. The lowest-lying one is denoted as ψ_t^{RM}. The function $\phi^{CM}(n_x, n_y, n_z)$ describes the solutions for the CM of the atom pair in the three directions with $n_i = 0, 1, 2, \ldots$ [44]. In the isotropic lattice, the excited bound states are typically threefold degenerate because of the factorization of the potential along the three directions. In the following, we will denote the degenerate states with the compact notation $\phi_{iso}^{CM}(n_x, n_y, n_z)$ implying any permutation of $\{n_x, n_y, n_z\}$. A schematic drawing of the relevant states for the reported measurements can be found in Fig. 1(c) for the isotropic

case, with a_s varied in units of $a_h = \sqrt{\hbar/(m\omega)}$, where ω is the trap frequency. The results are similar for both models. Additional crossings that violate parity conservation and cannot give rise to RM-CM coupling are not included in Fig. 1(c).

The experimental procedures are similar for both setups, and we give details here only for $E1$. We start from a Cs BEC of $\sim 3 \times 10^4$ atoms [47,48] with a condensate fraction of 70% to 80%, levitated against gravity by a magnetic field gradient $|\nabla B| \approx 31$ G/cm and held in a crossed optical dipole trap (XODT) at $\lambda = 1064.5$ nm generated by beams along the horizontal x and y directions. The trap depth of the XODT is $V_{trap} = k_B \times 0.29$ μK with trapping frequencies $\nu_x = 10.6(1.2)$ Hz, $\nu_y = 16.0(1.7)$ Hz, and $\nu_z = 20.8(1.5)$ Hz, where z denotes the vertical direction along gravity.

We load the BEC into a 3D cubic 1064-nm lattice with a depth of up to $V_{x,y,z} = 20.0(3)$ E_R, where E_R is the Cs recoil energy, by ramping up the power in the lattice beams within 500 ms. Together with a fine adjustment of the XODT to control the chemical potential, this creates a Mott insulator with predominant single-site occupancy [42,44]. Note that the finite size and finite temperature are responsible for some defects in the Mott insulator, including double occupancy of some sites. The offset magnetic field B is subsequently increased from $B_i = 21.0$ G to a value B_0 between 40 G and 100 G, while adjusting $|\nabla B|$ to keep the atoms levitated. In this interval, a_s varies in the range from $\sim 1.0 \times 10^3$ a_0 to $\sim 1.5 \times 10^3$ a_0, where a_0 is the Bohr radius, skipping the narrow FRs. We hold the atoms in the lattice for a time $\tau_h = 15$ to 20 ms. After τ_h, we reverse the procedure above. We image the atoms after 52 ms time of flight and we record the atom number N and the rms radius σ of the sample.

With $E1$ we observe four characteristic heating features, see Fig. 2(a). We attribute the feature P_0 to the FR at 47.8 G. The resolution is not sufficient to allow for the observation of substructure near this FR. The much narrower FR at 53.8 G does not show up in the data. The features P_1, P_2, and P_3 at $B = 56.5(2)$ G, 65.3(3) G, and 93.0(2) G, respectively, do not correspond to known FRs. In fact, they are ICIRs, as confirmed below. In $E2$, we tune a_s on the repulsive side of the FR at 47.8 G. This time we observe four atom-loss features P'_{1A}, P'_{1B}, P'_2, and P'_3 as B is scanned from 46 G to 47.6 G as shown in Fig. 2(b). We convert B into a_s according to Fig. 1(a) and plot both datasets together in Fig. 3. The positions of the heating features P_1, P_2, and P_3 agree reasonably well with the positions of the loss features P'_{1A} and P'_{1B}, P'_2, and P'_3, respectively. We attribute loss and heating features to the effect of holding the atoms near resonance. As discussed below, in $E2$ the feature P_1 from $E1$ appears to be split into two components P'_{1A} and P'_{1B}. We ascribe the splitting to some slight anisotropy of the lattice in $E2$ [44]. Features P'_2 and P'_3 are significantly broader than P_2 and P_3,
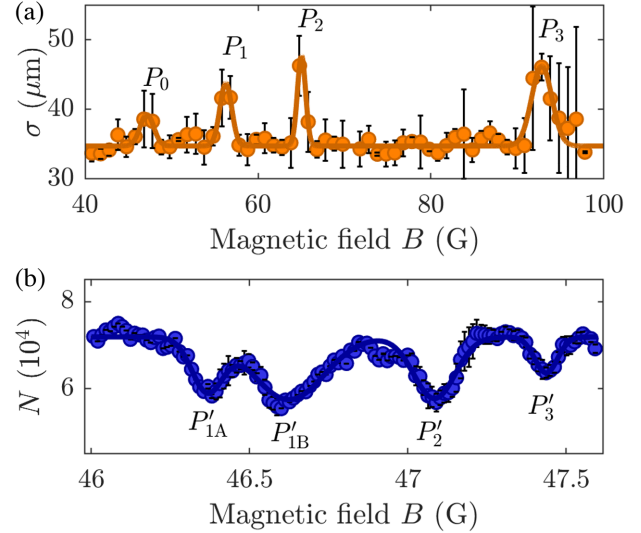

FIG. 2. Observation of ICIRs in a 3D lattice at $V_{x,y,z} = 20.0(3)$ E_R. (a) Cloud radius σ as a function of B for $E1$ after 20 ms hold time. The data are fit by a multipeak Gaussian (solid line) to guide the eye. (b) Atom number N as a function of B for $E2$ after 50 ms hold time, showing four loss features P'_j, $j = 1A$, 1B, 2, 3. The solid line is also a multipeak Gaussian fit. The error bars in both plots reflect the standard deviation from typically three experimental runs.

respectively. We attribute the broadening to the magnetic field gradient, which causes a spread of a_s across the sample [44]. This becomes increasingly larger as one climbs up the narrow FR at 47.8 G.

We now compare the experimental data with the predictions of the two models, without any fitting parameters. Even though the models are quite different, they both reflect the data reasonably well. The positions of P_1 and P_2 are in good agreement with the avoided crossings predicted by $M2$ of the state $\psi_t^{RM}\phi_{iso}^{CM}(0,0,0)$ with the threefold degenerate states $\psi_b^{RM}\phi_{iso}^{CM}(2,2,0)$ and $\psi_b^{RM}\phi_{iso}^{CM}(4,0,0)$, respectively. The difference in energy between the two states (2,2,0) and (4,0,0) stems from anharmonic corrections and hence leads to two different ICIRs. In Fig. 3 we indicate the calculated positions of the resonances from $M2$ and the intervals from $M1$. For P_1 and P_2 we again find reasonable agreement. We want to stress that the observed resonances arise from states in which two atoms initially occupy the same lattice site. Within the here prepared Mott insulator state, this situation can arise due to thermal excitations or imperfect preparation. If both atoms occupy the lowest energy state of the same lattice well, the relevant crossing for our model is to be expected with the state $\psi_t^{RM}\phi_{iso}^{CM}(0,0,0)$. It is interesting to note that, on the basis of our modeling, P_3 cannot arise from a crossing in which this state is involved. However, this resonance could be the result of further excitations in the Mott-insulator state. The avoided crossings of $\psi_t^{RM}\phi_{iso}^{CM}(2,0,0)$
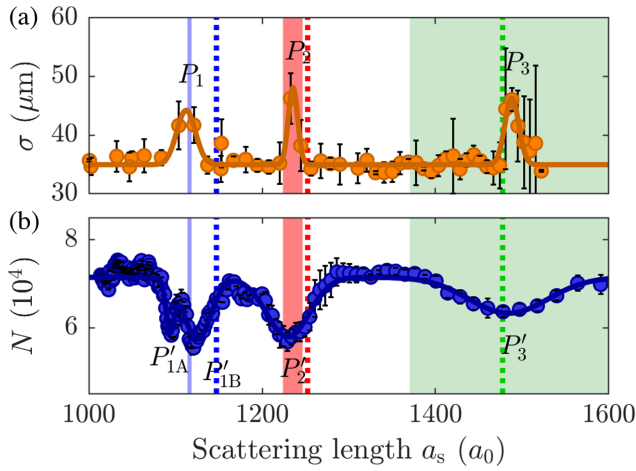
FIG. 3. Comparison of the data from the two experiments. (a) Cloud radius σ from $E1$ and (b) atom number N from $E2$ as a function of a_s. The resonance positions a_r are found at 1112(22) a_0, 1236(11) a_0, and 1488(16) a_0 for P_1, P_2, and P_3, respectively, and at 1094(10) a_0, 1124(26) a_0, 1266(40) a_0, and 1484(92) a_0 for P'_{1A}, P'_{1B}, P'_2, and P'_3, respectively. For each peak, the resonance position is obtained as the center of a Gaussian fit, the number in parenthesis indicates the width from the gaussian fit. The colored areas indicate the intervals obtained from $M1$, and the dotted lines represent the positions of the crossings as given by $M2$: $\psi_t^{RM}\phi_{iso}^{CM}(0,0,0)$ with $\psi_b^{RM}\phi_{iso}^{CM}(2,2,0)$ (blue) and with $\psi_b^{RM}\phi_{iso}^{CM}(4,0,0)$ (red), and $\psi_t^{RM}\phi_{iso}^{CM}(2,0,0)$ with $\psi_b^{RM}\phi_{iso}^{CM}(6,0,0)$ (green). The width of the blue area has been increased by a factor of 20 to improve visibility.
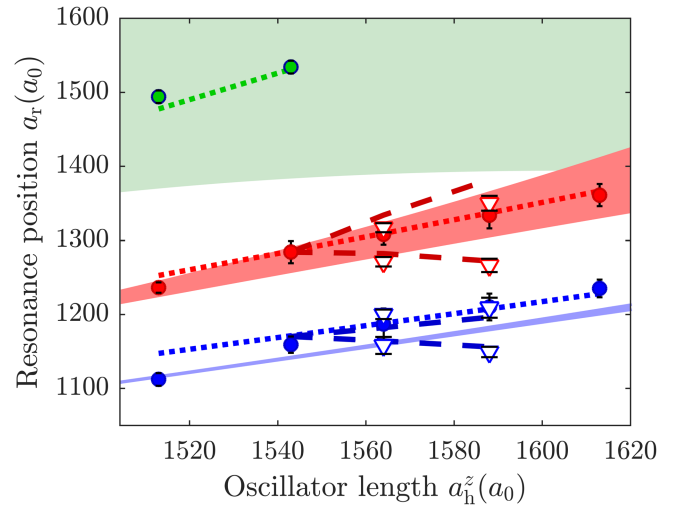

FIG. 4. Tuning of the ICIRs. Resonance position a_r for P_1 (blue), P_2 (red), and P_3 (green) as a function of the oscillator length a_h^z along the z direction for the isotropic (circles) and the anisotropic (triangles) case. For the isotropic case, $V_x = V_y = V_z$ was set to 20.0(3),18.5(3),17.5(3),16.5(3), and 15.5(3) E_R for the data from left to right. For the anisotropic case, $V_x = V_y = 18.5(3)$ E_R was chosen for $V_z = 17.5(3)$ E_R (left triangles) and 16.5(3) E_R (right triangles). The results from $M1$, applicable to the isotropic case, are shown as the blue, red, and green areas. The blue area has been widened by a factor of 3 to improve visibility. The predictions of $M2$ are plotted as dotted (dashed) lines for the isotropic (anisotropic) case.

with $\psi_b^{RM}\phi_{iso}^{CM}(6,0,0)$, and $\psi_t^{RM}\phi_{iso}^{CM}(1,0,0)$ with $\psi_b^{RM}\phi_{iso}^{CM}(5,0,0)$ are in fact very close to the position of P_3. We hypothesize that such excitations can be brought about by mixing of the lowest band with excited bands due to the strong interparticle interaction. In our case, the on-site interaction energy is $\sim$78% of the band gap to the first-excited lattice band [44], which may open the route for a non-negligible population of the excited states, i.e., bands, in a fully correlated many-body description.

Next, we test how the stiffness of the lattice confinement and the introduction of some controlled anisotropy affect the resonances, i.e., how their positions are tuned and to what extent they split. Within $E1$ we first vary $V_{x,y,z}$ in the range between 20.0(3) and 15.5(3) E_R while maintaining $V_x = V_y = V_z$. In Fig. 4 we plot the resulting resonance position a_r, obtained in the same way as for the resonances shown in Fig. 3, as a function of the harmonic oscillator length $a_h^z = \sqrt{\hbar/(m\omega_z)}$ along the z direction. As can clearly be seen for P_1 and P_2, the position shifts to higher values for a_r with increasing a_h^z. For P_3 only two data points are available, but also here a trend to higher values is present. For two specific values $V_z = 17.5(3)$ E_R and 16.5(3) E_R we then set $V_x = V_y = 18.5(3)$ E_R. The degeneracy is removed [44] by increasing a_h^z with respect to $a_h^{x,y}$. Here, the crossings of, e.g., $\psi_t^{RM}\phi^{CM}(0,0,0)$ with

$\psi_b^{RM}\phi^{CM}(2,0,2)$ and $\psi_b^{RM}\phi^{CM}(0,2,2)$ are found at the same position, but they are at a different position with respect to the crossing of $\psi_t^{RM}\phi^{CM}(0,0,0)$ with $\psi_b^{RM}\phi^{CM}(2,2,0)$. In such an anisotropic case, P_1 and P_2 split into two components, similarly to what we had observed earlier with $E2$. The splitting depends on the difference in the trapping potential along the three directions. Model $M1$, which takes into account the full lattice in the treatment of the CM [44], allows us to provide a range [49] within which the resonances for the isotropic case are more likely to be found. This turns out to be very narrow for P_1 and increasingly larger for P_2 and P_3 due to the increasing bandwidth of the lattice bands. Overall, the results of the models $M1$ and $M2$, with $M2$ addressing also the anisotropic case, are in fair agreement with the experimental data. Furthermore, the results are also supported by the double-well description within $M2$, see Ref. [44].

While in this Letter the positions and physical origin of the ICIRs, found experimentally to occur in strong 3D confinement, are well explained by the theoretical models, the details of how the resonance leads to loss and heating need further theoretical and experimental investigation. In particular, the degree of suppression of the loss features in the Mott-insulator state and the possible role of inhomogeneities, allowing for superfluid regions in the system, is

unclear. Studies of the loss dynamics and in particular of its density dependence would help elucidate the nature of the observed resonances, with connections to recent observations of tunneling dynamics of doublons in the regime of strong interactions and under strong three-body losses [50]. Three-body losses have not been considered explicitly in any of our theoretical models, where the loss was attributed to a two-step process via the creation of a mobile molecule, in analogy with previous observation in 1D geometry [30]. In this context, detecting the ICIRs out of a two-atom Mott-insulator shell could greatly elucidate the relevant processes.

Our results contribute to the understanding and characterization of CIRs, with prospects for the association of dimers in optical lattices [42,51–53] and optical tweezers [54–56] in the absence of, e.g., magnetic FRs, as a detection tool with potential implications in novel quantum sensors or as a step for creating ultracold molecules. In addition, these results add constraints for the stability of atoms in optical lattices or tweezers (and tweezer arrays) and become very relevant in the presence of systems with a high number of FRs like lanthanide atoms [57,58], or large lattice depths as in the case of quantum-gas microscopy [59,60].

Note added.—Recently, Lee *et al.* [62] also reported on the observation of resonances caused by CM-RM coupling. Interaction tuning is reported in a quasi-one-dimensional lattice, in contrast to losses measured for a three-dimensional lattice in the present work. A key difference is that in [62] the resonant process involves states delocalized over more than one well, and thus requires at least a double-well description [44,63]. Further recent work by Pinksa *et al.* [64] reports on yet another type of resonance due to CM-RM coupling, this time involving an ion and a neutral atom.

The data that support the findings of this study are made publicly available by the authors at [61].

[1] C. Gross and I. Bloch, Quantum simulations with ultracold atoms in optical lattices, Science **357**, 995 (2017).

[2] J. J. García-Ripoll, P. Zoller, and I. J. Cirac, Quantum information processing with cold atoms and trapped ions, J. Phys. B **38**, S567 (2005).

[3] I. Bloch, J. Dalibard, and W. Zwerger, Many-body physics with ultracold gases, Rev. Mod. Phys. **80**, 885 (2008).

[4] A. Mitra, Quantum quench dynamics, Annu. Rev. Condens. Matter Phys. **9**, 245 (2018).

[5] O. Morsch and M. Oberthaler, Dynamics of Bose-Einstein condensates in optical lattices, Rev. Mod. Phys. **78**, 179 (2006).

[6] P. Windpassinger and K. Sengstock, Engineering novel optical lattices, Rep. Prog. Phys. **76**, 086401 (2013).

[7] C. Chin, R. Grimm, P. Julienne, and E. Tiesinga, Feshbach resonances in ultracold gases, Rev. Mod. Phys. **82**, 1225 (2010).

[8] M. Greiner, O. Mandel, T. Esslinger, T. Hänsch, and I. Bloch, Quantum phase transition from a superfluid to a Mott insulator in a gas of ultracold atoms, Nature (London) **415**, 39 (2002).

[9] O. Dutta, M. Gajda, P. Hauke, M. Lewenstein, D.-S. Lühmann, B. A. Malomed, T. Sowiński, and J. Zakrzewski, Non-standard Hubbard models in optical lattices: A review, Rep. Prog. Phys. **78**, 066001 (2015).

[10] G. C. Strinati, P. Pieri, G. Röpke, P. Schuck, and M. Urban, The BCS–BEC crossover: From ultra-cold Fermi gases to nuclear systems, Phys. Rep. **738**, 1 (2018).

[11] C. A. Regal, C. Ticknor, J. L. Bohn, and D. S. Jin, Creation of ultracold molecules from a Fermi gas of atoms, Nature (London) **424**, 47 (2003).

[12] J. Herbig, T. Kraemer, M. Mark, T. Weber, C. Chin, H.-C. Nägerl, and R. Grimm, Preparation of a pure molecular quantum gas, Science **301**, 1510 (2003).

[13] N. Balakrishnan, Perspective: Ultracold molecules and the dawn of cold controlled chemistry, J. Chem. Phys. **145**, 150901 (2016).

[14] T. Zelevinsky, S. Kotochigova, and J. Ye, Precision test of mass-ratio variations with lattice-confined ultracold molecules, Phys. Rev. Lett. **100**, 043201 (2008).

[15] M. A. Baranov, M. Dalmonte, G. Pupillo, and P. Zoller, Condensed matter theory of dipolar quantum gases, Chem. Rev. **112**, 5012 (2012).

[16] M. Olshanii, Atomic scattering in the presence of an external confinement and a gas of impenetrable bosons, Phys. Rev. Lett. **81**, 938 (1998).

[17] D. S. Petrov, M. Holzmann, and G. V. Shlyapnikov, Bose-Einstein condensation in quasi-2d trapped gases, Phys. Rev. Lett. **84**, 2551 (2000).

[18] T. Bergeman, M. G. Moore, and M. Olshanii, Atom-atom scattering under cylindrical harmonic confinement: Numerical and analytic studies of the confinement induced resonance, Phys. Rev. Lett. **91**, 163201 (2003).

[19] P. O. Fedichev, M. J. Bijlsma, and P. Zoller, Extended molecules and geometric scattering resonances in optical lattices, Phys. Rev. Lett. **92**, 080401 (2004).

[20] V. Peano, M. Thorwart, C. Mora, and R. Egger, Confinement-induced resonances for a two-component ultracold atom gas in arbitrary quasi-one-dimensional traps, New J. Phys. **7**, 192 (2005).

[21] S. Grishkevich and A. Saenz, Theoretical description of two ultracold atoms in a single site of a three-dimensional optical lattice using realistic interatomic interaction potentials, Phys. Rev. A **80**, 013403 (2009).

[22] H. P. Büchler, Microscopic derivation of Hubbard parameters for cold atomic gases, Phys. Rev. Lett. **104**, 090402 (2010).

[23] S. Sala, P.-I. Schneider, and A. Saenz, Inelastic confinement-induced resonances in low-dimensional quantum systems, Phys. Rev. Lett. **109**, 073201 (2012).

[24] S. Sala and A. Saenz, Theory of inelastic confinement-induced resonances due to the coupling of center-of-mass and relative motion, Phys. Rev. A **94**, 022713 (2016).

[25] B. Schulz, S. Sala, and A. Saenz, Resonances in ultracold dipolar atomic and molecular gases, New J. Phys. **17**, 065002 (2015).

[26] D. Xiao, R. Zhang, and P. Zhang, Confinement-induced resonance with weak bare interaction in a quasi $3+0$ dimensional ultracold gas, Few-Body Syst. **60**, 63 (2019).

[27] E. L. Bolda, E. Tiesinga, and P. S. Julienne, Ultracold dimer association induced by a far-off-resonance optical lattice, Phys. Rev. A **71**, 033404 (2005).

[28] P.-I. Schneider, S. Grishkevich, and A. Saenz, Ab-initio determination of Bose-Hubbard parameters for two ultracold atoms in an optical lattice using a three-well potential, Phys. Rev. A **80**, 013404 (2009).

[29] J. P. Kestner and L.-M. Duan, Anharmonicity-induced resonances for ultracold atoms and their detection, New J. Phys. **12**, 053016 (2010).

[30] S. Sala, G. Zürn, T. Lompe, A. N. Wenz, S. Murmann, F. Serwane, S. Jochim, and A. Saenz, Coherent molecule formation in anharmonic potentials near confinement-induced resonances, Phys. Rev. Lett. **110**, 203202 (2013).

[31] M. Troppenz, S. Sala, P.-I. Schneider, and A. Saenz, Inelastic confinement-induced resonances in quantum dots, arXiv:1509.01159.

[32] E. Haller, M. Gustavsson, M. J. Mark, J. G. Danzl, R. Hart, G. Pupillo, and H.-C. Nägerl, Realization of an excited, strongly correlated quantum gas phase, Science **325**, 1224 (2009).

[33] G. Zürn, F. Serwane, T. Lompe, A. N. Wenz, M. G. Ries, J. E. Bohn, and S. Jochim, Fermionization of two distinguishable fermions, Phys. Rev. Lett. **108**, 075303 (2012).

[34] E. Haller, M. Rabie, M. J. Mark, J. G. Danzl, R. Hart, K. Lauber, G. Pupillo, and H.-C. Nägerl, Three-body correlation functions and recombination rates for bosons in three dimensions and one dimension, Phys. Rev. Lett. **107**, 230404 (2011).

[35] W. Kao, K.-Y. Li, K.-Y. Lin, S. Gopalakrishnan, and B. L. Lev, Topological pumping of a 1D dipolar gas into strongly correlated prethermal states, Science **371**, 296 (2021).

[36] E. Haller, M. J. Mark, R. Hart, J. G. Danzl, L. Reichsöllner, V. Melezhik, P. Schmelcher, and H.-C. Nägerl, Confinement-induced resonances in low-dimensional quantum systems, Phys. Rev. Lett. **104**, 153203 (2010).

[37] The observation of loss features in the 1D-to-2D crossover regime [36] was originally interpreted as stemming from the ECIR and later recognized to originate from ICIRs [23,38].

[38] S.-G. Peng, H. Hu, X.-J. Liu, and P. D. Drummond, Confinement-induced resonances in anharmonic waveguides, Phys. Rev. A **84**, 043619 (2011).

[39] G. Lamporesi, J. Catani, G. Barontini, Y. Nishida, M. Inguscio, and F. Minardi, Scattering in mixed dimensions with ultracold gases, Phys. Rev. Lett. **104**, 153202 (2010).

[40] B. Fröhlich, M. Feld, E. Vogt, M. Koschorreck, W. Zwerger, and M. Köhl, Radio-frequency spectroscopy of a strongly interacting two-dimensional Fermi gas, Phys. Rev. Lett. **106**, 105301 (2011).

[41] M. Berninger, A. Zenesini, B. Huang, W. Harm, H.-C. Nägerl, F. Ferlaino, R. Grimm, P. S. Julienne, and J. M. Hutson, Feshbach resonances, weakly bound molecular states, and coupled-channel potentials for Cesium at high magnetic fields, Phys. Rev. A **87**, 032517 (2013).

[42] L. Reichsöllner, A. Schindewolf, T. Takekoshi, R. Grimm, and H.-C. Nägerl, Quantum engineering of a low-entropy gas of heteronuclear bosonic molecules in an optical lattice, Phys. Rev. Lett. **118**, 073201 (2017).

[43] M. J. Mark, F. Meinert, K. Lauber, and H.-C. Nägerl, Mott-insulator-aided detection of ultra-narrow Feshbach resonances, SciPost Phys. **5**, 55 (2018).

[44] See Supplemental Material at http://link.aps.org/supplemental/10.1103/PhysRevLett.131.213002 for the details.

[45] T. Bush, M. B. G. Englert, and K. Rzażewski, Two cold atoms in a harmonic trap, Found. Phys. **28**, 549 (1998).

[46] The numerical simulations for $M1$ have been carried out using Cesium atoms, while those for $M2$ have been conducted with Lithium, whose validity has been previously assessed by comparison with a Cesium experiment [23].

[47] T. Weber, J. Herbig, M. Mark, H.-C. Nägerl, and R. Grimm, Bose-Einstein condensation of Cesium, Science **299**, 232 (2003).

[48] T. Kraemer, J. Herbig, M. Mark, T. Weber, C. Chin, H.-C. Nägerl, and R. Grimm, Optimized production of a Cesium Bose-instein condensate, Appl. Phys. B **79**, 1013 (2004).

[49] The actual range is slightly larger due to the experimental uncertainties in, e.g., the laser intensities.

[50] M. J. Mark, S. Flannigan, F. Meinert, J. P. D'Incao, A. J. Daley, and H.-C. Nägerl, Interplay between coherent and dissipative dynamics of bosonic doublons in an optical lattice, Phys. Rev. Res. **2**, 043050 (2020).

[51] F. Meinert, M. J. Mark, K. Lauber, A. J. Daley, and H.-C. Nägerl, Floquet engineering of correlated tunneling in the Bose-Hubbard model with ultracold atoms, Phys. Rev. Lett. **116**, 205301 (2016).

[52] S. A. Moses, J. P. Covey, M. T. Miecnikowski, B. Yan, B. Gadway, J. Ye, and D. S. Jin, Creation of a low-entropy quantum gas of polar molecules in an optical lattice, Science **350**, 659 (2015).

[53] T. Rom, T. Best, O. Mandel, A. Widera, M. Greiner, T. W. Hänsch, and I. Bloch, State selective production of molecules in optical lattices, Phys. Rev. Lett. **93**, 073002 (2004).

[54] K. Wang, X. He, R. Guo, P. Xu, C. Sheng, J. Zhuang, Z. Xiong, M. Liu, J. Wang, and M. Zhan, Preparation of a heteronuclear two-atom system in the three-dimensional ground state in an optical tweezer, Phys. Rev. A **100**, 063429 (2019).

[55] J. T. Zhang, Y. Yu, W. B. Cairncross, K. Wang, L. R. B. Picard, J. D. Hood, Y.-W. Lin, J. M. Hutson, and K.-K. Ni,

Forming a single molecule by magnetoassociation in an optical tweezer, Phys. Rev. Lett. **124**, 253401 (2020).

[56] D. K. Ruttley, A. Guttridge, S. Spence, R. C. Bird, C. R. L. Sueur, J. M. Hutson, and S. L. Cornish, Formation of ultracold molecules by merging optical tweezers, Phys. Rev. Lett. **130**, 223401 (2023).

[57] A. Patscheider, B. Zhu, L. Chomaz, D. Petter, S. Baier, A.-M. Rey, F. Ferlaino, and M. J. Mark, Controlling dipolar exchange interactions in a dense three-dimensional array of large-spin fermions, Phys. Rev. Res. **2**, 023050 (2020).

[58] J. Kumlin, K. Jachymski, and H. P. Büchler, Beyond-mean-field corrections for dipolar bosons in an optical lattice, Phys. Rev. A **99**, 033622 (2019).

[59] M. Rispoli, A. Lukin, R. Schittko, S. Kim, M. E. Tai, J. Léonard, and M. Greiner, Quantum critical behaviour at the many-body localization transition, Nature (London) **573**, 385 (2019).

[60] E. Haller, J. Hudson, A. Kelly, D. A. Cotta, B. Peaudecerf, G. D. Bruce, and S. Kuhr, Single-atom imaging of fermions in a quantum-gas microscope, Nat. Phys. **11**, 738 (2015).

[61] Dataset is available via Zenodo at 10.5281/zenodo.7108194.

[62] Y. K. Lee, H. Lin, and W. Ketterle, preceding Letter, Spin dynamics dominated by resonant tunneling into molecular states, Phys. Rev. Lett. **131**, 213001 (2023).

[63] F. Revuelta and A. Saenz, Inelastic confinement-induced resonances in multiwell potentials (to be published).

[64] M. Pinkas, O. Katz, J. Wengorowicz, N. Akerman, and R. Ozeri, Trap-assisted formation of atom–ion bound states, Nat. Phys. **19**, 1573 (2023).